

OFF-NUCLEAR STAR FORMATION AND OBSCURED ACTIVITY IN THE
LUMINOUS INFRARED GALAXY NGC 2623

A. S. EVANS,^{1,2} T. VAVILKIN,^{1,2} J. PIZAGNO,^{1,2} F. MODICA,¹ J. M. MAZZARELLA,³ K. IWASAWA,⁴ J. H. HOWELL,^{3,5}
J. A. SURACE,⁵ L. ARMUS,⁵ A. O. PETRIC,⁵ H. W. W. SPOON,⁶ J. E. BARNES,⁷ T. A. SUER,³
D. B. SANDERS,⁷ B. CHAN,³ AND S. LORD³

Received 2007 September 3; accepted 2008 January 24; published 2008 February 22

ABSTRACT

New optical *Hubble Space Telescope* (*HST*), *Spitzer Space Telescope*, and *XMM* observations of the luminous infrared galaxy (LIRG) NGC 2623 are presented. This galaxy was observed as part of the Great Observatories All-sky LIRG Survey (GOALS). The prominent 3.2 kpc southern extension to the nucleus has been resolved by *HST* observations into ~ 100 star clusters, making it one of the richest off-nuclear concentrations of bright clusters observed in GOALS. The clusters have $M_{F555W} \sim -6.6$ to -12.6 mag, which is within the magnitude range of Antennae galaxy clusters and in excess of 30 Doradus clusters at the high end. Their optical colors are primarily consistent with ages of ~ 1 – 100 Myr. Archival *GALEX* data show the off-nuclear region to be extremely bright in the far-ultraviolet, being equivalent in luminosity to the resolved nuclear region at $0.15 \mu\text{m}$, but becoming less energetically significant at increasing wavelengths. In addition, [Ne v] $14.3 \mu\text{m}$ emission is detected with *Spitzer* IRS, confirming the inference from the X-ray and radio data that an active galactic nucleus (AGN) is present. Thus, the off-nuclear optical clusters are associated with a secondary burst of activity corresponding to a star formation rate ~ 0.1 – $0.2 M_{\odot} \text{ yr}^{-1}$; the bulk of infrared (and thus bolometric) luminosity is generated via star formation and an AGN embedded behind dust within the inner kiloparsec of the system. If the infrared luminosity is primarily reprocessed starlight, the off-nuclear starburst accounts for $< 1\%$ of the present star formation in NGC 2623.

Subject headings: galaxies: active — galaxies: individual (NGC 2623) — galaxies: interactions —
infrared: galaxies

1. INTRODUCTION

Luminous infrared galaxy [LIRG; $L_{\text{IR}}(8\text{--}1000 \mu\text{m}) \geq 10^{11} L_{\odot}$] mergers are dynamically evolving galaxies that exhibit complex structure and harbor both obscured and unobscured starbursts and AGNs. As such, high-resolution observations that sample as much of the electromagnetic spectrum as possible are required to identify and reconstruct the distribution and luminosity of star-formation and AGN-related phenomena, as well as to probe the connection between merger state and the observed activity.

The present generation of space-based telescopes have the resolution, sensitivity, and collective wavelength coverage to make such studies a reality. As a first step toward a much larger multiwavelength study of LIRGs (i.e., the Great Observatories All-sky LIRG Survey, or GOALS), the present Letter focuses on NGC 2623 (= Arp 243, VV 079). The galaxy has an infrared (IR) luminosity of $L_{\text{IR}} = 3.3 \times 10^{11} L_{\odot}$ and a star-

forming molecular gas mass of $M_{\text{H}_2} \sim 8 \times 10^9 M_{\odot}$ (Bryant & Scoville 1999). Lack of strong $\text{H}\beta$ $\lambda 4861$ emission has hindered an accurate assessment of its optical emission line classification (e.g., Kim et al. 1995; Veilleux et al. 1995). Ground-based optical and near-IR images of the galaxy show it to be a prototypical, advanced merger—twin tidal tails extending from a single nucleus (e.g., Sanders et al. 2003; C. M. Ishida et al., in preparation). In this Letter, new high-resolution *HST* data are presented that show NGC 2623 to contain one of the richest and most compact off-nuclear regions of bright star clusters in the GOALS sample. New *XMM* and *Spitzer Space Telescope* data and archival *GALEX*, *Chandra X-Ray Observatory*, and VLA data are also presented in order to place the observed off-nuclear star formation within the framework of the total energy emanating from NGC 2623. Correcting the measured heliocentric radial velocity of NGC 2623 ($= 5549 \pm 1 \text{ km s}^{-1}$; Rothberg & Joseph 2006) for perturbations by the Virgo Cluster, the Great Attractor, and the Shapley Supercluster (Mould et al. 2000), then applying a cosmology with $H_0 = 73 \text{ km s}^{-1} \text{ Mpc}^{-1}$, $\Omega_m = 0.27$, and $\Omega_{\Lambda} = 0.73$ (Spergel et al. 2007), yields a luminosity distance of 77 Mpc and a scale of $0.36 \text{ kpc arcsec}^{-1}$.

2. OBSERVATIONS, DATA REDUCTION, AND RESULTS

Hubble Space Telescope observations of NGC 2623 with the Wide Field Channel (WFC) of the Advanced Camera for Surveys (ACS) were obtained on 2005 November 29 as part of a much larger campaign (A. S. Evans et al., in preparation) to image a complete sample of $88 L_{\text{IR}} \geq 10^{11.4} L_{\odot}$ IRAS galaxies in the Revised Bright Galaxy Sample (RBGS; Sanders et al. 2003). The galaxy was imaged with the F435W and F814W filters (approximately *B* and *I* bands) in a single orbit, with

¹ Department of Physics and Astronomy, Stony Brook University, Stony Brook, NY 11794-3800; aaron.evans@stonybrook.edu, tvavilk@vulcan.ess.sunysb.edu, jpizagno@zwicki.astro.sunysb.edu, matrix44474@aol.com.

² Visiting Astronomer, Infrared Processing and Analysis Center, California Institute of Technology, MS 100-22, Pasadena, CA 91125.

³ Infrared Processing and Analysis Center, California Institute of Technology, MS 100-22, Pasadena, CA 91125; mazz@ipac.caltech.edu, jhowell@ipac.caltech.edu, tsuer@ipac.caltech.edu, bchan@ipac.caltech.edu, lord@ipac.caltech.edu.

⁴ Max Planck Institute für Extraterrestrische Physik, Giessenbachstrasse, 85748 Garching, Germany; ki@mpe.mpg.de.

⁵ *Spitzer* Science Center, California Institute of Technology, Pasadena, CA 91125; jason@ipac.caltech.edu, lee@ipac.caltech.edu, andreea@ipac.caltech.edu.

⁶ Department of Astronomy, Cornell University, Ithaca, NY 14853; spoon@isc.astro.cornell.edu.

⁷ Institute of Astronomy, University of Hawaii, 2680 Woodlawn Drive, Honolulu, HI 96822; barnes@ifa.hawaii.edu, sanders@ifa.hawaii.edu.

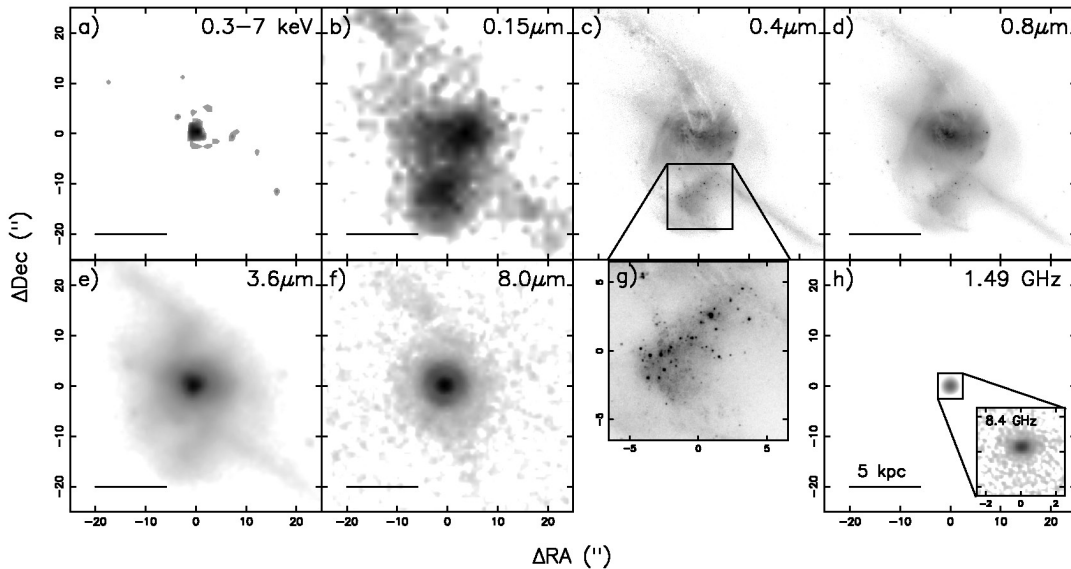


FIG. 1.—Multiwavelength view of the nuclear region of NGC 2623 displayed in order of increasing wavelength. The images have been spatially registered such that $\Delta R.A. = 0$ and $\Delta \text{decl.} = 0$ correspond to $R.A. = 08^{\text{h}}38^{\text{m}}24.1^{\text{s}}$, $\text{decl.} = +25^{\circ}45'16.4''$. The images shown are as follows: (a) *Chandra*, (b) *GALEX*, (c, d) *HST*, (e, f) *Spitzer*, (h) VLA. In all of the images, north is up and east is to the left.

integration times of 1275 and 730 s, respectively. A search through the *HST* archives also revealed a 1206-s, ACS-WFC F555W (approximately *V* band) observation; these data were retrieved to provide additional color information of the optically visible features. The *Spitzer* IRAC and MIPS observations were obtained on 2004 April 30 and 2004 December 3, respectively, as part of Guaranteed Time Observations (G. Fazio, PI). Integration times correspond to 144 s for the IRAC 3.6, 4.5, 5.8, and 8 μm channels and 42, 30, and 28 s for the MIPS 24, 70, and 160 μm channels, respectively. The *Spitzer* IRS short-high (SH) spectroscopic data were obtained on 2003 November 27 as part of Guaranteed Time Observations (J. Houck, PI); a 30 s ramp was taken with four cycles, for a total integration time of 252 s. The *HST* and *Spitzer* imaging and IRS data were reduced in the manner described in detail in A. S. Evans et al. (in preparation), J. M. Mazzarella et al. (in preparation), and L. Armus et al. (in preparation), respectively. The *GALEX* far- and near-ultraviolet (UV) data are archival and were first published in a *GALEX* atlas of nearby galaxies (Gil de Paz et al. 2007); the data set was reduced using the standard *GALEX* pipeline. Finally, *XMM* (EPIC pn) and archival *Chandra* X-ray data, the latter first published by Maiolino et al. (2003), were retrieved and analyzed. For the *Chandra* and *XMM* data, the integration times were 19.8 and 5 ks, respectively.

Figure 1 shows example images of the nuclear region of NGC 2623. The galaxy as a whole consists of northern and southern tidal tails, approximately 20–25 kpc in length, which extend from the nucleus in northeastern and southwestern arcs, respectively. A network of dust lanes, most prominent in the northern tail, continues along the position angle of the tidal tails into the high surface brightness nebular region of the nucleus. Bright, unresolved knots are distributed throughout the nuclear region; fainter knots are visible along the full length of both tails.

The most prominent feature in the *HST* images of NGC 2623 is a concentration of ~ 100 unresolved (i.e., ≤ 50 pc) knots embedded in a fan-shaped nebulosity which extends ~ 6 kpc to the southeast from the base of the southern tidal tail (Fig. 1g). These

knots have not been observed in prior ground-based images of the galaxy due to insufficient resolution of the observations (Rothberg & Joseph 2004; C. M. Ishida et al., in preparation). In addition, these knots are not resolved in the *GALEX* or *Spitzer Space Telescope* data; however, the fan-shaped nebulosity is visible in the far-UV and near-UV *GALEX* images (e.g., Fig. 1b), and in the 3.6 and 4.5 μm IRAC images (e.g., Fig. 1e).

The nuclear emission is resolved in the *GALEX*, *HST*, and shorter wavelength *Spitzer* IRAC images. At 8.0 μm and beyond, the bulk of the nuclear emission is concentrated in an unresolved core (Fig. 1f). The emission is unresolved in the longer (MIPS) wavelength *Spitzer* images, and the centroids are spatially aligned with the 8.0 μm core. The nuclear far-UV emission is offset from the 8.0 μm core and emanates primarily from the western half of the nucleus. Figure 1h shows 1.49 GHz and 8.4 GHz VLA images at 1.5'' and 0.25'' resolution, respectively (Condon et al. 1990, 1991). The 8.4 GHz emission is resolved and spatially aligned with the 8.0 μm core.

The X-ray emission observed with *Chandra* is compact; the image in the 2–7 keV band is nearly pointlike and its centroid coincides with the 8.0 μm core, while the soft band (0.4–2 keV) emission is resolved with the faint emission extending to 8'' from the nucleus. The 0.5–10 keV (up to 8 keV in the *Chandra* data) spectrum is hard (Fig. 2a); the photon index over this energy range is $\Gamma \sim 0.8$, but the data show some excess around 1 keV, characteristic of thermal emission of $T \sim 10^7$ K with contributions from Fe L emission lines. A similar Γ is derived with the *XMM* data. Maiolino et al. (2003) decomposed the *Chandra* spectrum into two components, deriving an absorbed $\Gamma \sim -0.3$ and a 2–10 keV luminosity $\sim 8 \times 10^{42}$ ergs s^{-1} (with an H I column density of $>10^{24}$ cm^{-2}). Given the *XMM* data quality, no attempt is made here to derive spectral parameters of a two-component fit. Regardless, the relevant fact is that the 2–10 keV *Chandra* and *XMM* spectra are extremely hard. The observed *Chandra* and *XMM* fluxes (and corresponding luminosities) are 1.3×10^{-14} ergs cm^{-2} s^{-1} (0.9×10^{40} ergs s^{-1}) in the 0.5–2 keV band and 1×10^{-13} ergs cm^{-2} s^{-1} (0.7×10^{41} ergs s^{-1}) in the 2–10 keV band.

Finally, multiple forbidden, H₂, and PAH emission lines are

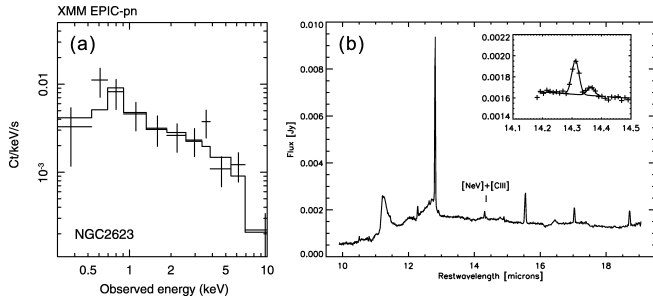


FIG. 2.—(a) *XMM-Newton* EPIC pn spectrum of NGC 2623. The spectral slope is approximately $\Gamma \approx 0.8$ over the whole energy range. The histogram shows the power law plus thermal emission fit. (b) *Spitzer* IRS spectrum of NGC 2623. The inset is centered on the [Ne v] 14.3 μm line; the fainter [Cl II] 14.4 μm line is also visible.

detected in the IRS spectrum (Fig. 2b), including the high ionization line [Ne v] 14.3 μm . The measured fluxes of [Ne v] and [Ne II] 12.8 μm are $(3.0 \pm 0.3) \times 10^{-17}$ and $(5.6 \pm 0.5) \times 10^{-16}$ W m^{-2} , respectively.

Accurate photometric measurements of the unresolved knots in the *HST* images require the removal of the nonuniform background of the underlying galaxy. Thus, the underlying galaxy was fit using the program Source Extractor (Bertin & Arnouts 1996) with a background mesh of 9 pixels \times 9 pixels. Once the background was removed, photometry of the knots was extracted using a modified version of the IDL routine APER (see F. Modica et al., in preparation).

3. DISCUSSION

As is apparent in the *HST* and *GALEX* images of NGC 2623, the galaxy has clear evidence of recent star formation. In the high-resolution *HST* images, the star formation that is most apparent is occurring in the largest and brightest of the asymmetries observed around the nucleus. While it is difficult to precisely determine the origin of this cluster-rich region without detailed modeling and kinematic data, two possibilities are that (1) it is part of a loop of material associated with the northern tidal tail (e.g., see Hibbard & Mihos 1995), or (2) it is nuclear tidal debris created during one of the final passages of the progenitor nuclei prior to their coalescence (Mihos & Hernquist 1996). Both scenarios can result in low velocity dispersions and thus Jeans instabilities that trigger star formation. In model 1, the inner loop of the tail is stretched via tides induced by the merger nucleus. In model 2, the leading edge of the region, which has overshot the nucleus during a close passage, is beginning its nuclear infall as the outer edge continues to move outward.

The star clusters within the off-nuclear region have absolute F555W magnitudes ($M_{\text{F555W}} = -6.6$ to -12.6 mag) within the range for clusters observed in the much closer and less luminous Antennae galaxy (NGC 4038/39; Whitmore et al. 1999). In addition, $\sim 7\%$ of the clusters have M_{F555W} in excess of the star-forming complex 30 Doradus ($M_V \sim -10.4$ mag). A comparison of the (F435W – F555W) and (F555W – F814W) colors of the clusters with the Bruzual & Charlot (2003) instantaneous burst population synthesis models shows the bulk of them to have ages of ~ 1 –100 Myr (i.e., assuming moderate to no extinction; Fig. 3). Further, the presence of strong UV emission from the off-nuclear region, which is comparable in far-UV brightness to the nucleus, is evidence of young OB stars, and thus constrains the age of most recent star formation to < 100 Myr. Better observational constraints on the cluster

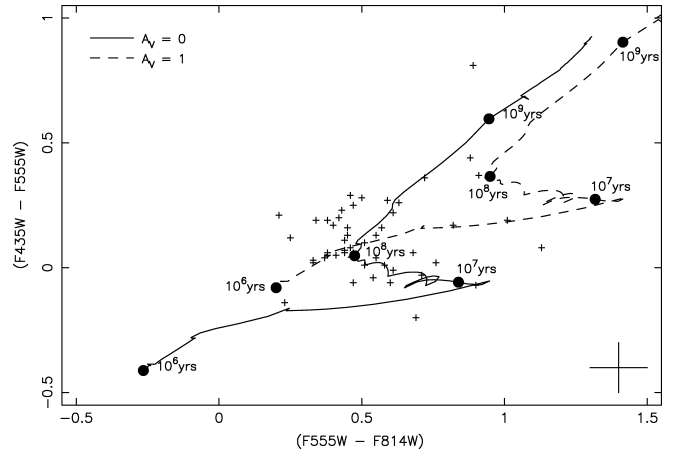


FIG. 3.—Color-color (F435W – F555W) vs. (F555W – F814W) diagram of the clusters in the off-nuclear star-forming region. Only clusters with both (F435W – F555W) and (F555W – F814W) uncertainties of < 0.11 mag are plotted (the maximum uncertainty is plotted as error bars on the lower right-hand side of the figure). The solid line represents the evolutionary track for an instantaneous burst computed using the GALAXEV (Bruzual & Charlot 2003) library of population synthesis models with solar metallicity, a Salpeter IMF with stellar mass range of 0.1–100 M_{\odot} , an age range of $10^{6.0}$ – $10^{9.7}$ yr, and an $A_V = 0$. The dashed line is the evolutionary track with an $A_V = 1$. Variations in metallicities and extinction toward the clusters contribute to the scatter observed in the diagram.

age-metallicity degeneracy that remains with broadband photometry will be provided by new high-resolution spectroscopy with the Keck Observatory (L. Chien, in preparation).

Although the physical mechanism responsible for the creation of the off-nuclear star-forming region in NGC 2623 is quite different from that of the Large Magellanic Cloud (LMC), the LMC provides a tangible comparison point of the size, brightness, and star formation rate of the off-nuclear region. The optical extent of the star-forming region (~ 3.2 kpc in diameter) is $\sim 60\%$ smaller than the LMC, and its M_{F555W} (-18.9 mag) is a factor of 2 brighter than the M_V of the LMC. The Galactic extinction-corrected UV luminosity of the off-nuclear region has been used to derive a star formation rate of 0.1–0.2 $M_{\odot} \text{ yr}^{-1}$, which is comparable to that estimated for the LMC (0.14) using H α as a star formation diagnostic (Kennicutt & Hodge 1986).

While the off-nuclear extension is nearly comparable in far-UV luminosity to the nucleus, and is clearly the site of the most prominent star formation in the *HST* images, these clusters are not simply the optically visible counterparts of a much more embedded and luminous ($\sim 10^{11} L_{\odot}$) off-nuclear starburst.⁸ The *Spitzer*, *Chandra*, and radio data show that the bulk of the emission from NGC 2623 emanates from the nuclear regions, and that the off-nuclear extension accounts for a decreasing amount of the total emission of the merger at longer wavelengths relative to the nucleus; the ratio of the emission from the southern extension relative to the nucleus decreases from ~ 0.8 in the far-UV to ~ 0.05 at 4.5 μm (as measured in a 14" diameter aperture centered on the nucleus and the center of the southern extension). From the extent of the high-resolution radio data (Fig. 1h) and the CO(1 \rightarrow 0) emission (i.e., the molecular gas; see Bryant & Scoville 1999), we conclude that the energetic nuclear region is no larger than ~ 600 –700 pc.

⁸ Off-nuclear, IR-bright star-forming regions have been observed in several LIRGs, most notably NGC 4038/39 and II Zw 096 (Mirabel et al. 1998; Goldader et al. 1997).

The nuclear luminosity of NGC 2623 has contributions from both star-formation and AGN activity. Brandl et al. (2006) use *Spitzer* low-resolution IRS data to show that NGC 2623 has a large $6.2\ \mu\text{m}$ PAH equivalent width ($=0.6\ \mu\text{m}$) and $6\text{--}15\ \mu\text{m}$ versus $15\text{--}30\ \mu\text{m}$ flux density ratios consistent with its being starburst-dominated at mid-IR wavelengths. However, NGC 2623 has a relatively deep silicate absorption feature and a derived optical depth at $9.8\ \mu\text{m}$ of $\tau_{9.8} \sim 1.5$ (Brandl et al. 2006), which is indicative of the source(s) of the bulk of the IR emission being partially hidden at mid-IR wavelengths. The galaxy clearly harbors an AGN; the $14.3\ \mu\text{m}$ [Ne v] emission line, which is only observed in galaxies hosting AGN, is present in the high-resolution IRS spectrum of NGC 2623 shown in Figure 2*b*. The observed ratio of [Ne v] to the low-ionization $12.8\ \mu\text{m}$ [Ne II] line is low (~ 0.05) relative to luminous AGN hosts such as Mrk 463E, Mrk 1014, and IRAS 05189–2524 (~ 1 ; see Armus et al. 2007), but similar to that of NGC 6240 (Armus et al. 2006). Thus, if the simplistic assumption is made that the extinction toward the observed [Ne v]- and [Ne II]-emitting regions are comparable, the AGN is energetically weak relative to the starburst population. This result is consistent with the high-resolution ($0.05''\text{--}0.15''$) $1.6\ \text{GHz}$ VLBI observations (Lonsdale et al. 1993) of NGC 2623; the data show a high brightness temperature ($T_b \gg 10^7\ \text{K}$) core, characteristic of an AGN, which only accounts for 9% of the total nuclear radio emission. The bulk of the radio emission is extended, and the observed $1.49\text{--}8.4\ \text{GHz}$ spectral index of $\alpha = 0.58$ ($f_\nu \propto \nu^{-\alpha}$) indicates (nonthermal) synchrotron emission, but without more information these data cannot be used to distinguish between an AGN (e.g., unresolved jets) or supernovae in an extended starburst. In terms of the X-ray data, the flat spectrum shown in Figure 2*a* supports the interpretation by Maiolino et al. (2003) that an obscured AGN may be present.⁹ In addition,

⁹ Obscured AGNs have also been observed in several luminous galaxies, including NGC 4945, NGC 6240, and UGC 5101 (Iwasawa et al. 1993; Vignati et al. 1999; Imanishi et al. 2003).

galaxies hosting obscured AGNs are sometimes observed to have apparent hard ($2\text{--}10\ \text{keV}$) X-ray to far-IR luminosity ratios less than the average ratio for H II region-dominated galaxies ($L_X/L_{\text{FIR}} \sim 10^{-3.7}$; Ranalli et al. 2003); this is also the case for NGC 2623 ($L_X/L_{\text{FIR}} \sim 6 \times 10^{-5}$). If the observed X-ray emission is primarily reflection of a Compton-thick AGN, the intrinsic X-ray emission would be suppressed by a factor of at least $10\text{--}1000$, thus lowering the intrinsic L_X/L_{FIR} from the range of $\sim 0.001\text{--}1$ occupied by classical QSOs and radio galaxies (e.g., see Evans et al. 2005).

Thus, NGC 2623 is a galaxy in which the concentration of prominent, off-nuclear clusters visible in the *HST* images constitute a secondary burst of activity generating $0.1\text{--}0.2\ M_\odot\ \text{yr}^{-1}$ of star formation, with the bulk of the IR (and thus bolometric) luminosity emanating from the inner kiloparsec of the nucleus. The total star formation of NGC 2623 as traced by the far-UV is $\sim 0.5\text{--}0.9\ M_\odot\ \text{yr}^{-1}$. In contrast, if star formation is responsible for the bulk of the dust heating, the far-IR or radio luminosities can be used to estimate nuclear star formation rates of $\sim 50\text{--}90\ M_\odot\ \text{yr}^{-1}$. At such a rate, the remaining lifetime of the luminous IR phase is, at most, $10^8\ \text{yr}$, i.e., the timescale for nuclear concentration of molecular gas to be consumed by star formation. The degree to which the AGN contributes to the observed activity of NGC 2623 is unclear; however, even if the AGN accounts for half of the L_{IR} of NGC 2623, the nucleus would still account for $>99\%$ of the star formation in the merger.

A. S. E. thanks G. Soutchkova, A. Gil de Paz, C. Mihos, J. Carpenter, J. Williams, J. Condon, D. Frayer, and F. Walter for useful discussions and assistance. Support for this work was provided by NASA through grant HST-GO10592.01-A from the Space Telescope Science Institute, which is operated by AURA, Inc., under NASA contract NAS5-26555. This research has made use of NED, which is operated by the JPL, California Institute of Technology, under contract with NASA.

REFERENCES

- Armus, L., et al. 2006, *ApJ*, 640, 204
 ———. 2007, *ApJ*, 656, 148
 Bertin, E., & Arnouts, S. 1996, *A&AS*, 117, 393
 Brandl, B. R., et al. 2006, *ApJ*, 653, 1129
 Bruzual, G., & Charlot, S. 2003, *MNRAS*, 344, 1000
 Bryant, P. M., & Scoville, N. Z. 1999, *AJ*, 117, 2632
 Condon, J. J., Helou, G., Sanders, D. B., & Soifer, B. T. 1990, *ApJS*, 73, 359
 Condon, J. J., Huang, Z.-P., Yin, Q. F., & Thuan, T. X. 1991, *ApJ*, 378, 65
 Evans, A. S., Mazzarella, J. M., Surace, J. A., Frayer, D. T., Iwasawa, K., & Sanders, D. B. 2005, *ApJS*, 159, 197
 Gil de Paz, A., et al. 2007, *ApJS*, 173, 185
 Goldader, J. D., Goldader, D. L., Joseph, R. D., Doyon, R., & Sanders, D. B. 1997, *AJ*, 113, 1569
 Hibbard, J. E., & Mihos, J. C. 1995, *AJ*, 110, 140
 Imanishi, M., Terashima, Y., Anabuki, N., & Nakagawa, T. 2003, *ApJ*, 596, L167
 Iwasawa, K., et al. 1993, *ApJ*, 409, 155
 Kennicutt, R. C., Jr., & Hodge, P. W. 1986, *ApJ*, 306, 130
 Kim, D.-C., Sanders, D. B., Veilleux, S., Mazzarella, J. M., & Soifer, B. T. 1995, *ApJS*, 98, 129
 Lonsdale, C. J., Smith, H. E., & Lonsdale, C. J. 1993, *ApJ*, 405, L9
 Maiolino, R., et al. 2003, *MNRAS*, 344, L59
 Mihos, J. C., & Hernquist, L. 1996, *ApJ*, 464, 641
 Mirabel, I. F., et al. 1998, *A&A*, 333, L1
 Mould, J. R., et al. 2000, *ApJ*, 529, 786
 Ranalli, P., Comastri, A., & Setti, G. 2003, *A&A*, 399, 39
 Rothberg, B., & Joseph, R. D. 2004, *AJ*, 128, 2098
 ———. 2006, *AJ*, 131, 185
 Sanders, D. B., Mazzarella, J. M., Kim, D.-C., Surace, J. A., & Soifer, B. T. 2003, *AJ*, 126, 1607
 Spergel, D. N., et al. 2007, *ApJS*, 170, 377
 Veilleux, S., Kim, D.-C., Sanders, D. B., Mazzarella, J. M., & Soifer, B. T. 1995, *ApJS*, 98, 171
 Vignati, P., et al. 1999, *A&A*, 349, L57
 Whitmore, B. C., et al. 1999, *AJ*, 118, 1551